

# The Silicon Vertex Detector of the Belle II Experiment

2 J. Wiechczynski,<sup>r,\*</sup> K. Adamczyk,<sup>r</sup> H. Aihara,<sup>p</sup> S. Bacher,<sup>r</sup> S. Bahinipati,<sup>e</sup>  
 3 J. Baudot,<sup>d</sup> P. K. Behera,<sup>f</sup> S. Bettarini,<sup>j,k</sup> T. Bilka,<sup>b</sup> A. Bozek,<sup>r</sup> F. Buchsteiner,<sup>a</sup>  
 4 G. Casarosa,<sup>j,k</sup> L. Corona,<sup>k</sup> S. B. Das,<sup>g</sup> G. Dujany,<sup>d</sup> C. Finck,<sup>d</sup> F. Forti,<sup>j,k</sup>  
 5 M. Friedl,<sup>a</sup> A. Gabrielli,<sup>l,m</sup> B. Gobbo,<sup>m</sup> S. Halder,<sup>i</sup> K. Hara,<sup>q,n</sup> S. Hazra,<sup>i</sup>  
 6 T. Higuchi,<sup>o</sup> C. Irmler,<sup>a</sup> A. Ishikawa,<sup>q,n</sup> Y. Jin,<sup>m</sup> M. Kaleta,<sup>r</sup> A. B. Kaliyar,<sup>a</sup>  
 7 J. Kandra,<sup>b</sup> K. H. Kang,<sup>o</sup> P. Kodyš,<sup>b</sup> T. Kohriki,<sup>q</sup> R. Kumar,<sup>h</sup> K. Lalwani,<sup>g</sup>  
 8 K. Lautenbach,<sup>c</sup> R. Leboucher,<sup>c</sup> J. Libby,<sup>f</sup> L. Martel,<sup>d</sup> L. Massaccesi,<sup>j,k</sup>  
 9 G. B. Mohanty,<sup>i</sup> S. Mondal,<sup>j,k</sup> K. R. Nakamura,<sup>q,n</sup> Z. Natkaniec,<sup>r</sup> Y. Onuki,<sup>p</sup>  
 10 F. Otani,<sup>o</sup> A. Paladino,<sup>A,j,k</sup> E. Paoloni,<sup>j,k</sup> K. K. Rao,<sup>i</sup> I. Ripp-Baudot,<sup>d</sup> G. Rizzo,<sup>j,k</sup>  
 11 Y. Sato,<sup>q</sup> C. Schwanda,<sup>a</sup> J. Serrano,<sup>c</sup> T. Shimasaki,<sup>o</sup> J. Suzuki,<sup>q</sup> S. Tanaka,<sup>q,n</sup>  
 12 F. Tenchini,<sup>j,k</sup> R. Thalmeier,<sup>a</sup> R. Tiwary,<sup>i</sup> T. Tsuboyama,<sup>q</sup> Y. Uematsu,<sup>p</sup> L. Vitale,<sup>l,m</sup>  
 13 Z. Wang,<sup>p</sup> H. Yin,<sup>a</sup> L. Zani<sup>B,c</sup> and F. Zeng<sup>o</sup> (Belle-II SVD collaboration)

14 <sup>a</sup>Institute of High Energy Physics, Austrian Academy of Sciences, 1050 Vienna, Austria

15 <sup>b</sup>Faculty of Mathematics and Physics, Charles University, 121 16 Prague, Czech Republic

16 <sup>c</sup>Aix Marseille Université, CNRS/IN2P3, CPPM, 13288 Marseille, France, <sup>B</sup>presently at INFN Sezione di  
 17 Roma Tre, I-00185 Roma, Italy

18 <sup>d</sup>IPHC, UMR 7178, Université de Strasbourg, CNRS, 67037 Strasbourg, France

19 <sup>e</sup>Indian Institute of Technology Bhubaneswar, Bhubaneswar 752050, India

20 <sup>f</sup>Indian Institute of Technology Madras, Chennai 600036, India

21 <sup>g</sup>Malaviya National Institute of Technology Jaipur, Jaipur 302017, India

22 <sup>h</sup>Punjab Agricultural University, Ludhiana 141004, India

23 <sup>i</sup>Tata Institute of Fundamental Research, Mumbai 400005, India

24 <sup>j</sup>Dipartimento di Fisica, Università di Pisa, I-56127 Pisa, Italy, <sup>A</sup>presently at INFN Sezione di Bologna,  
 25 I-40127 Bologna, Italy

26 <sup>k</sup>INFN Sezione di Pisa, I-56127 Pisa, Italy

27 <sup>l</sup>Dipartimento di Fisica, Università di Trieste, I-34127 Trieste, Italy

28 <sup>m</sup>INFN Sezione di Trieste, I-34127 Trieste, Italy

29 <sup>n</sup>The Graduate University for Advanced Studies (SOKENDAI), Hayama 240-0193, Japan

30 <sup>o</sup>Kavli Institute for the Physics and Mathematics of the Universe, University of Tokyo, Kashiwa 277-8583,  
 31 Japan

32 <sup>p</sup>Department of Physics, University of Tokyo, Tokyo 113-0033, Japan

33 <sup>q</sup>High Energy Accelerator Research Organization (KEK), Tsukuba 305-0801, Japan

34 <sup>r</sup>H. Niewodniczanski Institute of Nuclear Physics, Krakow 31-342, Poland

35 E-mail: wiechczynski@belle2.ifj.edu.pl

---

\*Speaker

36 The Belle II experiment operating at the asymmetric-energy  $e^+e^-$  SuperKEKB collider, located in Tsukuba (Japan), has been collecting data since March 2019. Its excellent vertexing abilities are provided by the vertex detector, part of which is the silicon-strip vertex detector (SVD) that plays a crucial role in the charged-particle tracking close to the interaction point. The SVD has operated successfully and efficiently over the whole period of data taking so far. In this article, we briefly discuss its purpose, structure and basic description of the front-end electronics. The main quantities related to the SVD performance are presented. The foreseen increase in SuperKEKB luminosity will lead to higher background, so we describe its impact on the SVD performance. A quick overview of the radiation damage campaign is presented to show the predicted behaviour of the sensors subjected to high radiation, whose level is constantly monitored. We also discuss the ongoing software development to account for the high occupancy expected in the future. In particular, the utilization of the SVD hit time information is presented as a very important quantity to suppress off-time background hits and tracks. Finally, the work done during the first long shutdown of SuperKEKB is briefly described, during which a major upgrade of the pixel detector has been successfully done. Resumption of the beam operation is expected in early 2024.

Keywords: Silicon strip detector, Vertex detector, Tracking detector, Belle II

## 1. Introduction

The Belle II [1] experiment is dedicated to search for physics beyond the standard model at the intensity frontier. It operates at the SuperKEKB collider located at KEK, Tsukuba in Japan, providing asymmetric beams of 7 GeV electrons and 4 GeV positrons. In the accelerator's default operation regime, the center-of-mass energy is set to the  $\Upsilon(4S)$  resonance, hence it produces a huge sample of  $B$  mesons via the  $e^+e^- \rightarrow \Upsilon(4S) \rightarrow B\bar{B}$  process. So far, SuperKEKB achieved the highest instantaneous luminosity of  $4.7 \times 10^{34} \text{ cm}^{-2}\text{s}^{-1}$ , which is the current world record. The Belle II detector is a multipurpose spectrometer characterized by excellent vertexing capability and good hermeticity, which has accumulated  $424 \text{ fb}^{-1}$  to date, and its final goal is to collect a data sample of  $50 \text{ ab}^{-1}$ , that will be possible with a constant increase of the SuperKEKB instantaneous luminosity up to our final goal of  $6 \times 10^{35} \text{ cm}^{-2}\text{s}^{-1}$ .

Belle II is composed of various sub-detectors with the vertex detector (VXD) being the closest to the interaction point. It is divided into two further subsystems. The innermost part is the pixel detector (PXD), which is based on depleted field effect transistor pixel sensors. The PXD consists of two layers (numbered 1-2) and its main goal is the precise determination of the decay vertices. Outside the PXD is the silicon-strip vertex detector (SVD) [2] with four layers (numbered 3-6) that mostly extrapolates the measured tracks to the PXD, defining the so-called region of interest (ROI), which significantly reduces the amount of data recorded by the PXD. The SVD also performs standalone tracking for low-momentum charged particles and contributes to their identification by providing energy loss information.

## 2. SVD structure

Each SVD layer is composed of a number of double-sided silicon strip detectors (DSSDs) that are manufactured on an n-type bulk wafer with a thickness of about  $300 \mu\text{m}$  (Figure 1). One side of the sensor is covered by the p-type silicon strips placed in parallel to the beam axis that determine the  $r - \phi$  coordinates (distance from the  $z$ -axis and azimuthal angle, respectively), and the n-type strips are placed perpendicularly on the other side of the bulk, measuring the  $z$  coordinate (collinear to the electron beam). Figure 1 (left) shows a schematic picture of SVD layers and associated sensors with increasing numbering from the forward (FWD) to the backward (BWD) regions. Such structure is repeated along the azimuthal direction forming different ladders and the so-called windmill geometry of the SVD. The sensors differ depending on the layer and the region in which they are placed in the SVD. In the FWD part, for layers 4-6, they have a trapezoidal shape

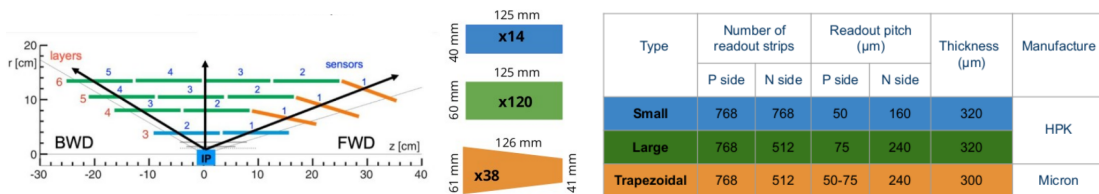


**Figure 1:** Schematic picture of SVD sensors forming different layers (left) and a table summarizing the parameters for each type of sensor (right).

68 and are slanted in the region that, due to the asymmetric beams, is characterised by the highest track  
69 multiplicity. In addition, in layer 3 the sensors are smaller and contain more n-type strips than that  
70 in layers 4-6. This also implies the readout pitch (distance between two readout strips) to be much  
71 smaller for p-side strips with respect to the n-side. To improve spatial resolution, a floating strip is  
72 placed between two readout strips on both p- and n-sides. The charge induced in the floating strip  
73 is shared by the neighboring strips, reducing the effective strip pitch to half of the readout pitch.  
74 The right table of Figure 1 summarises the sensor parameters. The SVD consists of 224 thousand  
75 readout strips and 172 sensors with an active area of 1.2 m<sup>2</sup>.

## 76 2.1 Front-end electronics

77 For the readout we use APV25 chips [3]. For the central part of SVD (except for layer 3), the  
78 chips are attached directly to the DSSD sensors via flex circuits bent over the DSSD edge (Origami  
79 concept). The edge sensors use hybrid boards located outside the active volume. The APV25 has  
80 128 channels per chip and amplifiers that provide a shaping time of 50 ns. Radiation hardness  
81 exceeds 100 Mrad and the power consumption is around 0.4 W/chip. The sampling frequency is 32  
82 MHz and after the trigger's arrival we can collect six consecutive signal samples in total with the  
83 multipeak mode. To account for higher luminosity in the future, we have introduced the so-called  
84 "3/6 mixed acquisition mode", which allows switching between three and six samples recorded on  
85 an event-by-event basis, based on the trigger type (and hence its time accuracy) for a particular  
86 event. This mode, already prepared and tested, significantly reduces the data size, which can be  
87 crucial in high background conditions.

## 88 3. SVD performance

89 Since the start of the operation we have observed very smooth performance of the SVD, with a  
90 very few masked strips (less than 1%). Moreover, the environment has been stable and the evolution  
91 of calibration constants is consistent with expectation. Also, the effects of radiation damage are  
92 well under control.

93 Several quantities related to the SVD performance - sensor efficiency, signal-to-noise ratio, and  
94 both spatial and time resolution - are constantly monitored. Regarding SVD sensor efficiency, the  
95 values for all sensors are typically over 99% and they are also very stable over the whole period of  
96 data taking. Clusters are formed from adjacent strips with significant signal and the charge collected  
97 in a given cluster strongly depends on the incident angle of the track. Over time, we observe very  
98 similar cluster charge in all the sensors once normalized to the track's length. For layer 4-5-6 on  
99 the n-type strips we observe 10-30% loss of the signal due to the large pitch combined with the  
100 presence of a floating strip. Another important quantity is the signal-to-noise ratio (SNR), which is  
101 satisfactory for all 172 sensors. The SNR MPV is ranging from 13 to 30, depending on the sensor  
102 position, due to the track incident angle with the sensor, and on the sensor side, with smaller SNR  
103 for the p-sides, due to larger noise for the longer strip length. A small decrease of cluster SNR value  
104 is observed in 2022 measurement, due to increased noise from radiation damage by approximately  
105 20%-30%. In Figure 2 the distributions of cluster charge (left) and SNR (right) are presented,  
106 where histograms representing the data collected in 2020 and 2022 are superimposed.

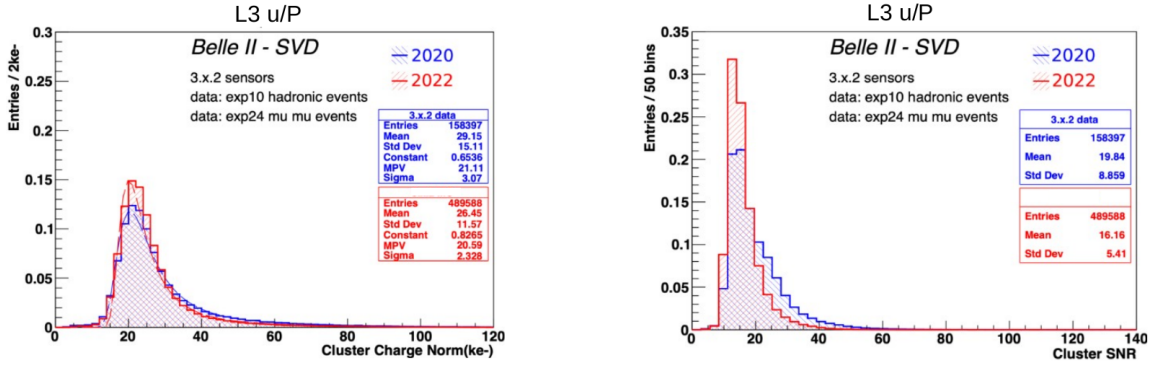


**Figure 2:** Distribution of cluster charge (left) and signal-to-noise ratio (right) for layer 3 (p-side). Comparison between data taken in 2020 (blue) and 2022 (red) is presented.

107 Both position and time resolution are very important metrics for excellent SVD performance.  
 108 The position resolution measurement is based on the residuals, i.e., the clusters' positions with  
 109 respect to the intercept of the unbiased tracks' extrapolation, and it is evaluated with a large sample  
 110 of  $e^+e^- \rightarrow \mu^+\mu^-$  decays. As shown in Figure 3, this quantity depends on the incident angle and is  
 111 very stable during the period of the Belle II operation. Cluster position is calculated as the center  
 112 of gravity (i.e. weighted mean) of the various strip positions inside the cluster, using the collected  
 113 charge as strip weight. The cluster position resolution then depends on cluster size and on the  
 114 strip signal-to-noise ratio, varying with the track incident angle with an expected non monotone  
 115 dependence visible in Figure 3. For zero incident angle, with perpendicular tracks more likely to  
 116 produce a single strip cluster, one can only achieve a "digital" resolution, corresponding to the  
 117 standard deviation of a flat distribution inside implanted strip pitch (floating strip pitch/ $\sqrt{12}$ ). The  
 118 resolution improves with more than one strip in the cluster, adding the center of gravity analog  
 119 information. It reaches a minimum for two strip clusters, corresponding to the incident angle for  
 120 which the projection of the track along the direction perpendicular to the strips on the detector  
 121 plane is two floating strip pitches (4 and 14 degrees for the layer 3 p- and n-sides pitches). For  
 122 large incident angle, since the signal collected in each strip decreases with the incident angle  $\theta$   
 123 (proportional to pitch/ $\sin(\theta)$ ), the consequent reduction of the strip signal-to-noise ratio degrades  
 124 the cluster position resolution, visible in Figure 3. In general, the resolution for the n-side (right  
 125 plot) is about two times worse with respect to that for the u-side, which is a result of the different  
 126 pitch and strip signal-to-noise ratio on the two sides.

127 Hit time resolution is measured with respect to the event time of the collision provided by  
 128 central drift chamber (CDC) and exhibits a very good resolution of less than 3 ns for the clusters  
 129 associated to tracks. Using the average value of all the hits on a given track, the so-called "track-  
 130 time" can be computed, slightly improving the time resolution. Furthermore, the "event-time"  
 131 can be determined using all the clusters associated to selected tracks in an event. In such a way,  
 132 the "event time" can be computed by the SVD with a resolution of the order of 1 ns, while the  
 133 computation is around 2000 times faster than the one based on CDC. This feature will be especially  
 134 important in the higher luminosity environment, as it can significantly speed up the reconstruction  
 135 process at the high-level trigger.

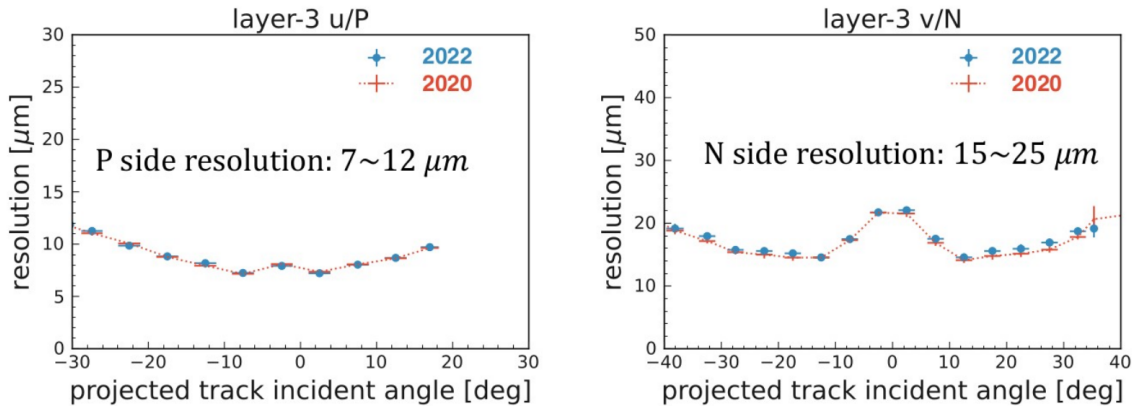


**Figure 3:** Distributions of position resolution for *p*-side (left) and *n*-side (right) as a function of the track incident angle. A comparison between data taken in 2020 (dots) and 2022 (dotted lines) is presented.

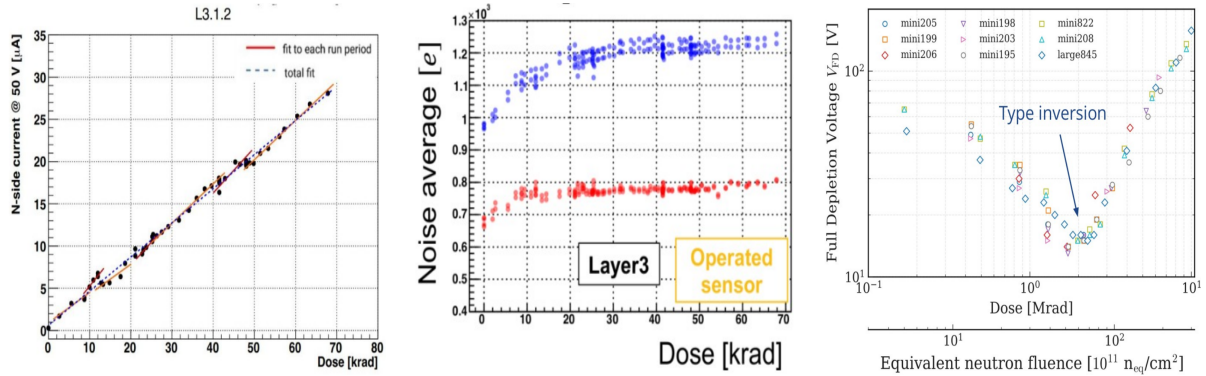


**Figure 4:** Left plot: Leakage current as a function of the accumulated dose; Center plot: the average noise level as a function of the accumulated dose for the *p*-side (blue dots) and *n*-side (red dots); Right plot: full depletion voltage as a function of the accumulated dose with the type inversion observed at 2 Mrad.

#### 136 4. Radiation effects

137 In the high-energy physics experiments, the effects from radiation damage coming from ma-  
 138 chine related background is a major factor that **degrades** the sensor performance with time. The  
 139 SVD accumulated dose is constantly measured using data from diamond sensors that are mounted  
 140 on the IP beam pipe, and the corresponding level of the equivalent neutron fluence is evaluated using  
 141 the ratio of equivalent neutron fluence to dose estimated from Monte Carlo simulation. Several  
 142 effects related to radiation damage must be taken into account. A linear increase of the leakage  
 143 current as a function of radiation damage is observed in the sensors, as expected from the bulk  
 144 damage described by the NIEL model [4], and shown in Figure 4 left. The sensor current is shown  
 145 as a function of the accumulated dose for one of the layer 3 sensors most exposed, that received  
 146 about 70 krad to date, corresponding to an equivalent neutron fluence of about  $1.6 \times 10^{11} \text{ n}_{\text{eq}}/\text{cm}^2$ .  
 147 So far, this increase has had a negligible contribution to the noise because of both the small leakage



148 current and the short APV25 shaping time. The rate of the leakage current increase measured  
149 is consistent with the experience from other experiments working with similar detectors and in  
150 comparable conditions [5]. However, we expect some significant impact on the strip noise due to  
151 the sensor leakage current, and hence a deterioration in SNR, for the dose of  $\sim 6$  Mrad, which is  
152 considered as SVD dose limit to preserve optimal performance. The strip noise for unirradiated  
153 modules is dominated by the interstrip capacitance. During the operation we have observed an  
154 increase in its value of about 20% (30%) for n-side (p-side), due to effects of surface radiation  
155 damage that increases the interstrip capacitance, but it is expected to saturate, as also visible in  
156 Figure 4 center.

157 Another relevant effect of the bulk radiation damage is the impact on depletion voltage.  
158 The expected future radiation levels at the nominal luminosity, of about 0.35 Mrad/year and  $8 \times$   
159  $10^{11}$   $n_{\text{eq}}/\text{cm}^2/\text{year}$ , are affected by large uncertainty due to the machine evolution as well as a  
160 possible redesign of the interaction region. To better explore the possible effects of bulk damage in  
161 the SVD sensors after bulk type inversion, an irradiation campaign was conducted in July 2022 at  
162 ELPH, Tohoku University. Several SVD sensors have been exposed to a 90 MeV electrons beam,  
163 up to 10 Mrad, corresponding to an equivalent neutron fluence of  $3 \times 10^{13}$   $n_{\text{eq}}/\text{cm}^2$ . The decrease  
164 of the depletion voltage has been observed up to the point of bulk type inversion, which occurred at  
165 2 Mrad ( $\sim 6 \times 10^{12}$   $n_{\text{eq}}/\text{cm}^2$ ), after which the depletion voltage started to increase again (Figure 4  
166 right). Detailed measurements, whose results will be shortly published, confirmed that the sensors  
167 will still work fine after the type inversion, which meets our expectation for these types of silicon  
168 detectors. Since the beginning of the detector operation, we have not observed any change in the  
169 depletion voltage in the sensors installed in the SVD, as expected due to the small accumulated  
170 equivalent neutron fluence so far, below  $2 \times 10^{11}$   $n_{\text{eq}}/\text{cm}^2$ . Considering all these results, the dose  
171 limit of 6 Mrad and the extrapolation of the background levels quoted above, the SVD has a wide  
172 safety margin for the accumulated radiation damage even after 10 years of the operation at the target  
173 luminosity.

## 174 5. High background scenario and related software/hardware developments

175 With the increase of the luminosity and the expected larger machine related background, the  
176 SVD occupancy will also increase and a deterioration of the tracking performance is expected above  
177 certain levels. So far, the average hit occupancy is 0.5% for layer 3, which does not degrade the  
178 performance. Nonetheless, the background extrapolation for different future scenarios has been  
179 performed with detailed simulations of the various contributions (beam-gas, Toushek, etc.) and  
180 applying appropriate data-simulation scale factors [6]. These studies predict that for the nominal  
181 luminosity we can reach an occupancy in layer 3 very close to the limit of 4.7%, above which the  
182 tracking performance deteriorates. These predictions have large uncertainties coming from poorly  
183 known machine evolution in the future, with a possible redesign of the interaction region. In the  
184 most conservative scenario, the layer-3 occupancy can increase up to  $\sim 8.7\%$ , which is far beyond  
185 the modest tracking performance. Such a scenario motivates us to develop the SVD reconstruction  
186 software, as well as to seriously consider the VXD upgrade [7], since the safety factor might be too  
187 small to ensure good quality data. The technology assessment related to this hardware upgrade is  
188 currently ongoing.

189 An important effort related to the software development is the utilization of the hit time  
190 information from the SVD. The real signal hits come from well-triggered collisions, but the SVD  
191 acquisition window ( $\sim 100$  ns) is much wider with respect to the SuperKEKB bunch spacing (6 ns).  
192 Therefore, we need to cope with many off-time hits related to the beam-induced background or  
193 background from the other bunches. The current selection is based on two requirements: a) time  
194 difference between p- and n-side cluster,  $|t_p - t_n| < 20$  ns, and b) the absolute value of the cluster  
195 time,  $|t_{p,n}| < 50$  ns. These criteria reject the majority of the background hits retaining above 99% of  
196 the signal, and based on them the SVD occupancy limit for layer 3 can be set at 4.7%. Recently, a  
197 more effective background suppression method has been developed in the form of so-called “SVD  
198 grouping”. It is based on an event-by-event classification of the clusters by their time, so the  
199 clusters belonging to tracks from the same collisions are collected in the same group. Clusters  
200 from the different collisions or beam background will be placed in the other groups; finally, only  
201 the clusters belonging to the priority group will be used for the tracking. This feature reduces the  
202 fake rate (fraction of the fake tracks) by 16% for the high-background scenario. An additional fake  
203 rate reduction can be achieved by applying the selection on the track-time to reject off-time tracks.  
204 Finally, these improvements allow an increase of the SVD occupancy limit for layer 3 from 4.7% to  
205 around 6%.

## 206 6. Activities during the Long Shutdown 1

207 Long shutdown 1 (LS1) started in May 2022 and one of the goals was to upgrade the VXD with a  
208 new PXD. During the first data taking period, the second layer of PXD was only partially equipped,  
209 and 5/6 of the azimuthal angle remained uncovered. The new PXD provides the full coverage,  
210 which is beneficial for more precise vertexing. Hardware activities for the VXD uninstallation and  
211 reinstallation were intense: after the VXD extraction from Belle II, the SVD was detached from  
212 the old PXD (May 16-17, 2023), then the new PXD was attached to the SVD (June 20-21, 2023)  
213 and finally the complete VXD was installed in the Belle II detector. The whole delicate procedure  
214 had neither major problems nor caused any damage. In the period of September 12 - October 1,  
215 2023, the VXD commissioning was performed to confirm the PXD and SVD performance, and  
216 also to check the impact from the increased PXD power consumption and possible increase in  
217 the temperature on the sensor leakage current. From September 21, several cosmic runs with no  
218 magnetic field were taken to check the performance and compare them with corresponding ones  
219 for 2022 data samples. We observed no issues, in particular the noise distributions over readout  
220 channels remained basically unchanged as well as SNR for the clusters associated to the tracks, with  
221 stable excellent efficiency for all the sensors.

## 222 7. Conclusions

223 To conclude, SVD has successfully operated since March 2019 with very smooth performance  
224 and without major problems. Its good vertexing quality has been confirmed by many physics  
225 measurements, in particular those related to the lifetime analyses e.g. Ref. [8]. Some radiation  
226 damage effects were observed, but without any impact on the performance so far.



227 However, the extrapolated background level indicates that the occupancy in the SVD can exceed  
228 the current limit that **guarantees** good tracking performance. Hence, several software improvements  
229 are being implemented to account for high background conditions. In particular, exploitation of  
230 the SVD hit time is of major importance. Alongside, a VXD upgrade is also under discussion to  
231 increase robustness against high background and to match a possible new interaction region.

232 The VXD reinstallation at Belle II with complete PXD has been successfully done during the  
233 LS1, followed by successful VXD commissioning with cosmic data. The beam operation is planned  
234 to resume in early 2024.

## 235 **References**

- 236 [1] T. Abe et al., Belle II Technical Design Report, arXiv:1011.0352 (2010).  
237 [2] K. Adamczyk et al., JINST **17**, P11042 (2022).  
238 [3] M. J. French et al., Nucl. Instrum. Meth. A **466**, 359 (2001).  
239 [4] G. Lindstrom et al., Nucl. Instrum. Meth. A **465**, 60-69 (2000).  
240 [5] B. Aubert et al., Nucl. Instrum. Meth. A **729**, 615 (2013).  
241 [6] A. Natochii et al., Nucl. Instrum. Meth. A **1055**, 168550 (2023).  
242 [7] M. Babeluk et. al., Nucl. Instrum. Meth. A **1048**, 168015 (2023).  
243 [8] F. Abudinén et al., Phys. Rev. Lett. **130**, 071802 (2023)